Environmental Health Engineering and Management Journal 2023, 10(2), 165–177
http://ehemj.com

doi 10.34172/EHEM.2023.19

Environmental Health Engineering and Management Journal

Original Article

Open Access Publish Free

Activation of persulfate by TiO_2-Fe_3O_4 nanocomposite for reactive red 198 degradation along with modeling and optimization approach

Somayeh Rahimi[1], **Farzaneh Mohammadi**[2*], **Soudabeh Ghodsi**[2], **Maryam Mohammadi**[3], **Hossein Karimi**[2]

[1]Department of Environmental Health, Firoozabad Branch, Islamic Azad University, Firoozabad, Iran
[2]School of Health, Isfahan University of Medical Sciences, Isfahan, Iran
[3]Department of Management and Health Information Technology, School of Management and Medical Information Sciences, Isfahan University of Medical Sciences, Isfahan, Iran

Abstract

Background: Recently, sulfate radical-based photocatalytic processes have attracted significant interests because of unique advantages in pollutants purification. In this study, TiO_2-Fe_3O_4 nanocomposites in the presence of persulfate and under ultraviolet light-emitting diode (UV-LED) irradiation were applied for reactive red 198 removal with a focus on the main operating parameters such as pH, persulfate molar concentration, irradiation time, and catalyst dosages in different initial concentrations.

Methods: The nanoparticles were synthesized by co-precipitation technique. The X-ray diffraction (XRD), field emission scanning electron microscopy (FESEM) coupled with energy dispersive X-ray (EDX) and Fourier transform infrared spectroscopy (FTIR) analysis were used to evaluate TiO_2-Fe_3O_4 nanocomposites. The response surface methodology (RSM) was employed for modeling and optimization. The kinetics and mechanisms of decolorization by sulfate and hydroxyl radicals were investigated. The mineralization of dye was evaluated using total organic carbon (TOC) analysis.

Results: Modeling and optimization through RSM showed that the maximum decolorization of reactive red 198 is accursed an initial concentration of 10-50 mg/L was reached under UV-LED irradiation of 62-85 min, persulfate concentration = 0.8-1 mM, 0.19-0.3 g/L TiO_2-Fe_3O_4 nanocomposites concentration, and pH = 3. The kinetics of process was in agreement with pseudo-first order. The mineralization of reactive red 198 during the optimum conditions was determined at about 61.1% and 49.6%, meanwhile, the decolorization efficiency in the same conditions was approximately 98.1% and 87.6%, respectively.

Conclusion: The use of TiO_2-Fe_3O_4 nanocomposites under UV-LED irradiation in the presence of persulfate can be used as an efficient and promising method for dye removal from textile wastewater.

Keywords: Reactive red 198, Nanocomposites, Titanium dioxide, Wastewater

Citation: Rahimi S, Mohammadi F, Ghodsi S, Mohammadi M, Karimi H. Activation of persulfate by TiO_2-Fe_3O_4 nanocomposite for reactive red 198 degradation along with modeling and optimization approach. Environmental Health Engineering and Management Journal 2023; 10(2): 165–177. doi: 10.34172/EHEM.2023.19.

Article History:
Received: 3 July 2022
Accepted: 28 October 2022
ePublished: 25 April 2023

***Correspondence to:**
Farzaneh Mohammadi,
Email: fm_1363@hlth.mui.ac.ir

Introduction

In recent decades, with the increasing speed of urbanization and industrialization, a significant increase in wastewater production has been observed (1). Various harmful pollutants are produced as a result of the activities of industries such as plastic, textile, food, cosmetics, leather, printing, pharmaceuticals, and paint production, and can enter the environment through wastewater (2). The textile industry is one of the most effective industries in many countries. The discharge of textile industry wastewater into aquatic environments is one of the most important concerns of environmentalists. One of the most essential dangerous species in textile wastewater is dyes. These compounds have destructive effects on marine ecosystems. Dyes have a complex chemical structure and high molecular weight, which enter the environment due to various processes such as dyeing. The dyes include disperse, azo, acidic, basic, direct, mordant, sulfur and reactive dyes. Some dyes and their decomposition compounds are highly toxic, carcinogenic, and non-biodegradable (3). Therefore, effective treatment processes are essential for human health and the environment (4). So far, various methods such as coagulation and flocculation, reverse osmosis, ion exchange and absorption have been used to treat these wastewaters. Despite the relative success of each of these methods, due to the high stability of the constituents of these wastewaters, and also, in order to achieve higher standards, the necessity of using this alternative method with high efficiency is felt more. Among various treatment methods, advanced oxidation processes (AOPs) is considered as one of the best potential processes to treat pollutants, including the advantages such as the production of neutral and harmless products, rapid oxidation, and oxidation of low concentrations of pollutants (5).

The photocatalytic process is one of the methods of AOPs in which organic materials are decomposed under ultraviolet (UV) radiation and in the presence of metal dioxides (6). The mechanism of semiconductor photocatalysts starts with the irradiation of light on its surface, and during irradiation, due to the absorption of photons with energy equal to or greater than the energy gap of the photocatalyst, electrons are excited from the conduction band and lead to the formation of electron-hole pairs. With electron migration, the holes created on the surface of the photocatalyst react with water and oxygen molecules and cause the production of free radicals, which are the cause of pollutant destruction. Titanium dioxide (TiO_2) is a heterogeneous catalyst with three crystal structures including rutile, anatase, and brookite, and the highest photocatalytic activity is related to anatase and rutile. TiO_2 is widely used in organic pollutants removal from various environments because of its efficient photoactivity, safety, high stability, and low cost. Nonetheless, the main problem with TiO_2 is their separation from the solution after the treatment. One of the methods to solve this problem is doping magnetic materials in the nanocomposite structure, which can be easily separated from the solution using a magnet. Hence, Fe_3O_4 could be doped on semiconductors for this purpose. The presence of Fe_3O_4 could also increase the TiO_2 photocatalytic activity, based on the energy level theory (7,8).

Persulfate ($S_2O_8^{-2}$) is a new form of oxidants, which is used to substitute with common oxidants such as H_2O_2 and O_3 and in the AOPs. Persulfate (PS) is a powerful oxidant (2.1 V), which is decomposed under UV radiation and produced highly reactive, short-lived sulfate radicals ($SO4^{\circ-}$, 2.6 V). The benefits of persulfate-based AOPs are the capability to activate with different methods, good performance in a wide range of pH, achieve higher radical formation yield and lower maintenance, and transportation costs because of the accessibility of persulfate salts (9).

The studies have proved that the ultraviolet light-emitting diode (UV-LED) sources cause higher efficiency in AOPs and have some advantages such as low energy consumption, higher shock resistance, short operation time, and being environmentally friendly. Therefore, the use of UV-LED for the photocatalytic degradation of organic pollutants has been recently considered (10,11).

Many researchers have widely synthesized and applied TiO_2-Fe_3O_4 nanocomposites (TFNs) as a photocatalyst or adsorbent for removal of various contaminants. TFNs due to the presence of iron, are used for photocatalysis and PS activation. Also, TFNs are magnetically separable composite photocatalysts (12).

Response surface methodology (RSM) is a mathematical and statistical modeling method for developing experimental models, which requires two stages of experiment design and determination of an approximate function. RSM has a high ability to predict economic costs and time (13,14).

It should be noted that a few studies investigate the performance of TFNs along with persulfate and UV-LED irradiation. In addition, there is no study in which TFN along with persulfate have been used in the presence of UV-LED radiation to remove reactive red 198 (RR198) dye from the environment. Therefore, in this study, the synergistic decomposition of RR198 dye was investigated by TFNs + PS + UV-LED photoreactor. The most critical parameters evaluated are pH, PS molar concentration, irradiation time, and catalyst dosages in different initial concentrations. Subsequently, the RSM was used for modeling and optimization of the studied parameters. The central composite design (CCD) was applied for the experimental design. The kinetics, mechanisms and mineralization of the system were investigated.

Materials and Methods

Chemicals and materials

The Reactive Red 198 (CAS# 145017-98-7) was purchased from AlvanSabet Company (Iran). The dye characteristics are as below:

Color Index: C.I.Reactive Red 198; Color Index Number: 18221; Azo group: Single azo class; Type: Anionic; Molecular Formula: $C_{27}H_{18}C_1N_7Na_4O_{16}S_5$; λ_{max} (nm): 518; Molecular weight (g/mol): 968.21.

The other materials are titanium dioxide nanoparticles (CAS# 13463-67-7, Degussa Germany), sodium hydroxide, ferrous chloride ($FeCl_2{\cdot}6H_2O$), ferric chloride ($FeCl_3{\cdot}6H_2O$), and technical ethanol grade, 99% purchased from Merck (Darmstadt, Germany), and potassium persulfate (99%, Sigma-Aldrich, CAS# 7727-21-1).

Nanocomposite synthesize methodology and characteristics

The preparation of Fe_3O_4, the mixture of 50 mL of $FeCl_2.6H_2O$ (2 mol/L) and 50 mL of $FeCl_3.6H_2O$ (1 mol/L) was sonicated in an ultrasonic bath at 100 W for 20 minutes. Afterward, 25 mL of sodium hydroxide (1 mol/L) was poured into the solution, which led to the formation of the black precipitate, then, sonicated for 30 minutes at 60°C and separated within a 1.2 T magnet (Kanetec, Japan). To synthesize TFNs, Fe_3O_4, and TiO_2 nanoparticles were added into ethanol so that the Ti/

Fe and Fe^{2+}/Fe^{3+}ratios were 1/1 and 1/2, respectively. The suspension was sonicated at 100 W and 60°C for 35 minutes. Black precipitate was collected and put into the oven for 12 hours at 185°C. The powder was washed several times with ethanol and water, and then, calcined for 2 hours at 300oC (15,16).

The nanocomposite was characterized through field emission scanning electron microscopy (FESEM, MIRA3-FEG, US) equipped with an energy dispersive X-ray spectroscopy (EDX) adapter, which is a surface analytical technique. Fourier-transform infrared spectroscopic (FTIR) was applied to analyze the functional groups on the sample surface (Necolet 6700, USA). The crystal structures of the nanocomposite were determined using an X-ray diffraction pattern (XRD, diffractometer Bruker AXS D8, Germany).

Reactor Setup

A glass cylinder reactor was used for experiments with the effective volume of 500 mL (10 cm diameter, 12 cm height). One UV-LED light source (14W-KINGBO) was applied for the irradiation with a 395-400 nm wavelength. The ultraviolet irradiation was monitored by the ultrafast fiber optic spectrometer (AvaSpec-128, Avantes, the Netherlands). The distance between the UV-LED source and sample surface was 5 cm. The UV-LED lamp had an outer diameter of 9 cm consisting of 7 LED components, 2 watt each. The viewing angle was around 120°, so that the emitted radiation could cover the whole sample surface. The solution temperature was kept at about 25°C. The UV-LED reactor system is shown in Figure 1.

Photocatalysis experiments

The RR198 solution was added to the reactor with desired concentration. The solution pH was adjusted to the desired value using dilute NaOH and H2SO4 (1.0 M). Then, the TFNs was added to the solution, and after that, PS was added to the sample. To make the solution, homogenous magnetic stirrer was used and the sample was irradiated with a UV-LED source for different time intervals. Immediately after collecting the sample, sodium thiosulfate was added to quench any residual sulfate and hydroxyl radicals. Then, suspended nanocomposite particles were separated via centrifugation at 5000 rpm for 5 minutes followed by filtration through a 0.22 µm filter (17).

UV-Vis spectra for RR198 were recorded through a UV-Vis spectrophotometer (TU-1901). The RR198 dye concentration was determined through HACH DR 5000 spectrometer at 518 nm wavelength. Decolorization efficiency was obtained using Eq. (1).

$$\%\, dye\, removal = \frac{C_o - C_t}{C_o} \times 100 \qquad \text{Eq. 1}$$

Where C_0 is the initial concentration and C_t is the final concentration. The mineralization of RR198 was determined by measuring total organic carbon (TOC) through a TOC analyzer (Shimadzu).

Experimental design

For modeling and optimization of the RR198 removal efficiency, the RSM model was selected and implemented in Design-Expert 11 software. Here, five independent variables including initial concentration, solution pH, TFNs dosage, UV-LED irradiation time, and PS concentration were investigated. The RR198 removal percentage would be dependent on the response variable. The ranges and levels of the independent variables are demonstrated in Table 1. The CCD was applied for design of experiments. Finally, 45 tests (45 runs) were designed, which are represented in Table 2.

Table 1. Range of the studied variables

Parameters		Level				
		-2	-1	0	+1	+2
A	C_i-RR198 (mg/L)	10	20	30	40	50
B	pH	3	5	7	9	11
C	TFNs (g/L)	0.1	0.15	0.2	0.25	0.3
D	Time (min)	10	30	50	70	90
E	PS (mM)	0.2	0.4	0.6	0.8	1
Total number of experiments				45		

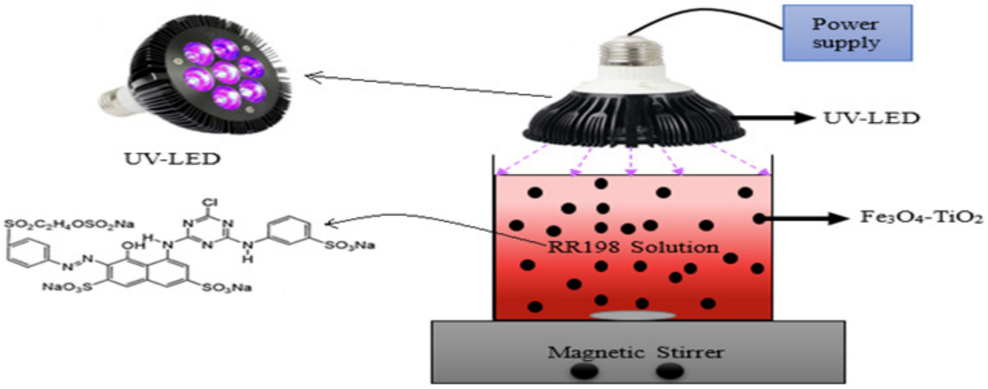

Figure 1. The schematic diagram of UV-LED reactor

Table 2. RSM-CCD experimental and predicted results

Run Order	RR198 Concentration	pH	TFNs	Time	PS	Actual value	Predicted value
	A	B	C	D	E		
1	10	7	0.2	50	0.6	54.32	55.36
2	20	5	0.15	30	0.4	45.32	42.07
3	20	5	0.25	30	0.4	55.48	57.27
4	20	5	0.15	30	0.8	51.38	54.18
5	20	5	0.25	30	0.8	69.64	69.38
6	20	9	0.15	30	0.4	18.34	17.96
7	20	9	0.25	30	0.4	19.15	18.04
8	20	9	0.15	30	0.8	24.38	25.03
9	20	9	0.25	30	0.8	26.13	25.12
10	20	5	0.15	70	0.4	62.12	57.43
11	20	5	0.25	70	0.4	71.12	72.64
12	20	5	0.15	70	0.8	71.16	69.54
13	20	5	0.25	70	0.8	83.16	84.74
14	20	9	0.15	70	0.4	23.18	25.04
15	20	9	0.25	70	0.4	25.68	25.12
16	20	9	0.15	70	0.8	29.95	32.12
17	20	9	0.25	70	0.8	31.67	32.2
18	30	7	0.2	10	0.6	25.64	25.37
19	30	3	0.2	50	0.6	78.54	79.62
20	30	7	0.2	50	0.2	40.73	38.78
21	30	7	0.1	50	0.6	28.37	29.78
22	30	7	0.2	50	0.6	51.87	55.63
23	30	7	0.2	50	0.6	55.67	55.63
24	30	7	0.2	50	0.6	57.24	55.63
25	30	7	0.3	50	0.6	55.17	51.66
26	30	7	0.2	50	1	58.12	57.97
27	30	11	0.2	50	0.6	13.89	10.71
28	30	7	0.2	90	0.6	45.33	43.5
29	40	5	0.15	30	0.4	28.35	28.51
30	40	5	0.25	30	0.4	45.34	50.31
31	40	5	0.15	30	0.8	43.19	40.62
32	40	5	0.25	30	0.8	66.87	62.41
33	40	9	0.15	30	0.4	12.47	12.14
34	40	9	0.25	30	0.4	13.57	18.81
35	40	9	0.15	30	0.8	18.33	19.22
36	40	9	0.25	30	0.8	26.38	25.89
37	40	5	0.15	70	0.4	37.42	39.57
38	40	5	0.25	70	0.4	63.15	61.36
39	40	5	0.15	70	0.8	47.16	51.67
40	40	5	0.25	70	0.8	74.38	73.46
41	40	9	0.15	70	0.4	16.12	14.91
42	40	9	0.25	70	0.4	19.97	21.58
43	40	9	0.15	70	0.8	23.87	21.99
44	40	9	0.25	70	0.8	26.17	28.66
45	50	7	0.2	50	0.6	41.4	38.26

The results of the experiments showed a high agreement with the quadratic RSM model (Eq. 2).

$$y=\beta_o+\sum_{i=1}^{k}\beta_i X_i+\sum_{i=1}^{k}\beta_{ii} X_i^{2}+\sum_{i=1}^{k}\sum_{i\neq j=1}^{k}\beta_{ij} X_i X_j+\varepsilon \qquad \text{Eq. 2}$$

Where y, $X_{i,j}$, k, β_0, β_i, β_{ii}, β_{ij}, and ε represent the predicted responses, encoded independent variables, number of variables, model constant, coefficients of linear variables, coefficients of second-order variables, coefficients of variables interactions, and the error rate, respectively (18,19).

In this study, the optimization module implemented in Design-Expert software was applied to optimize the studied variables. The target is to maximize the decolorization within the initial concentration range from low to high levels.

Results

Figures 2A and 2B show the FTIR spectra and XRD pattern of TiO_2, Fe_3O_4, and TFNs. FESEM images of Fe_3O_4, TiO_2, and TFNs are shown in Figure 2C. EDX analysis of TFNs is visible in Figure 2D. Figure 2E illustrates the UV-Vis absorption spectra at different irradiation times at 50 mg/L concentration and pH = 5 in the presence of TFNs and PS under UV-LED light.

The results of ANOVA in statistical analysis are represented in Table 3. Figure 3 demonstrated the diagnostic plots in the output of the RSM model. Figure 4A to 4C represent the RSM model response for studied variables. Figure 4E shows the optimized variables. Figure 5 stands for the degradation rate of RR198 in different conditions such as pH = 3, RR198 concentration = 50 mg/L, reaction time = 90 min. Figure 6 explains the mechanism of free radical production in UV-LED/TFNs/PS system. Figure 7 illustrates the linear regression of pseudo-first-order reaction kinetics at photocatalyst dosage 0.3 g/L, pH = 3, initial concentration = 50 mg/L, and time = 90 min. Also, the comparison of the performance of nanocomposites in different photocatalytic processes in the removal of dyes is presented in Table 4.

Discussion

TFNs characteristics

Figure 2A shows the FTIR spectra of TiO_2, Fe_3O_4, and TFNs. The FTIR spectra were obtained at a wavenumber range of 400–4000 cm^{-1} under ambient conditions. The TFNs absorption peaks demonstrated the combination of TiO_2 and Fe_3O_4 peaks. TFNs spectra show the O-H stretching vibration absorption peak at 3435 cm^{-1}, which is close to that for TiO_2 and Fe_3O_4 spectra at 3441 and 3413 cm^{-1}, respectively. Also, the presence of a peak at about 1630 cm^{-1} is arising from the hydroxyl groups. The stretching vibration at about 1043-1405 cm^{-1} indicates the presence of Ti–O and Fe–O–Ti bonds. The peak at around

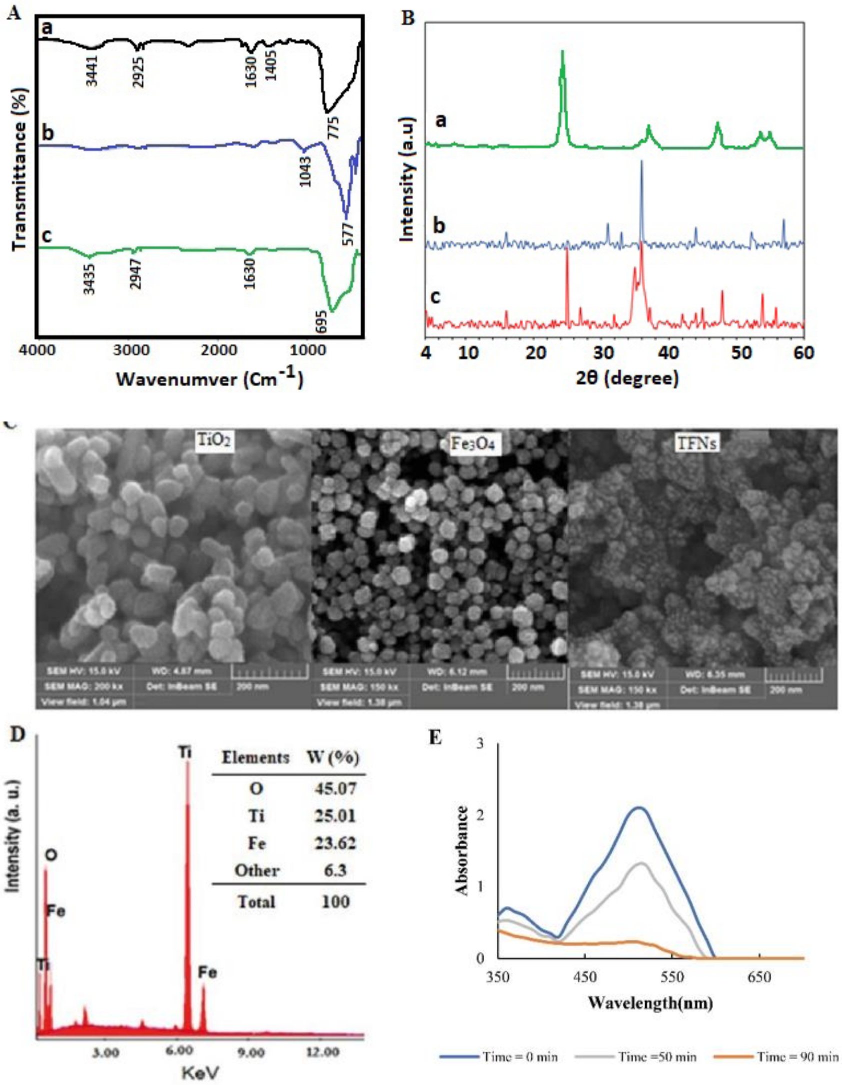

Elements	W (%)
O	45.07
Ti	25.01
Fe	23.62
Other	6.3
Total	100

Figure 2. (A) FTIR spectra; (B) XRD pattern; (C) FESEM images; (D) EDX analysis of TFNs; (E) UV-Vis absorption spectrum of the RR198 at different irradiation times (experimental conditions: RR198 = 50 mg/L, pH = 5, TFNs = 0.03 g/L, $S_2O_8^{2-}$ = 1 mM)

472-775 cm^{-1} shows the Ti-O-Ti bands, which is relatively more comprehensive due to the overlapping of Ti–O and Fe–O peaks, confirming the attachment of TiO_2 on the surface of Fe_3O_4 and successful TFNs synthesis (25).

The XRD pattern in the 2θ ranges of 4-60° was shown in Figure 2B. The XRD pattern of the TiO2 nanoparticles is shown in Figure 2B. The 2θ at peaks 25°, 37-38°, 48°, and 54-55° confirms the TiO2 anatase structure. Figure 2B represents a series of diffraction peaks at around 2θ of 31°, 33°, 36°, 44°, 53°, 57°, which are related to the planes of Fe_3O_4. The XRD pattern of TFNs in Figure 2B, indicates diffraction peaks at around 2θ of 25°, 35-37°, 48°, 54°, and 56° (15). In addition to the peaks from Fe3O4, there are the peaks of TiO2. The TFNs peak intensity and peak position in the XRD pattern demonstrate the crystalline photocatalyst structure (26).

The FESEM images of Fe_3O_4, TiO_2, and TFNs are shown in Figure 2C. TiO_2 nanoparticles are homogeneous in morphology and texture with a smooth surface, while some dots are visible in TFNs, which show the Fe_3O_4 nanoparticles. Fe_3O_4 nanoparticles formation is evident in Figure 2C. TiO_2 nanoparticles are somewhat larger than Fe_3O_4. The TFNs is still at the nanoscale and less than 100 nm.

An EDX spectrum are plotted in Figure 2D and identifies the elements corresponding to each of the peaks.

Here, it shows the presence of Ti and Fe in TFNs. The weight percentage of Ti 25.01% was approximately equal to Fe 23.62%, indicating the successful synthesis of TFNs, and no impurities were found in EDX mapping.

The absorption spectrum and photocatalytic decolorization of RR198

Figure 2E demonstrates the UV-Vis absorption spectra at different irradiation times at 50 mg/L concentration and pH = 5 in the presence of TFNs and PS under UV-LED light. The maximum absorption peak of RR198 is observed at 512 nm. Figure 2E shows that with the increase of time, the absorption peak intensity decreases because

Table 3. ANOVA results for quadratic RSM model

Source	Sum of squares	*df*	Mean square	F value	*P* value
Model	1.74	16	0.1086	123.77	<0.0001*
A-RR198 Con.	0.0731	1	0.0731	83.25	<0.0001*
B-pH	1.19	1	1.19	1352.85	<0.0001*
C-TFNs	0.1196	1	0.1196	136.26	<0.0001*
D-Time	0.0822	1	0.0822	93.66	<0.0001*
E-PS	0.0920	1	0.0920	104.80	<0.0001*
AB	0.0120	1	0.0120	13.65	0.0009*
AC	0.0087	1	0.0087	9.90	0.0039*
AD	0.0037	1	0.0037	4.23	0.0491*
BC	0.0457	1	0.0457	52.09	<0.0001*
BD	0.0137	1	0.0137	15.62	0.0005*
BE	0.0051	1	0.0051	5.77	0.0232*
A^2	0.0124	1	0.0124	14.17	0.0008*
B^2	0.0175	1	0.0175	19.95	0.0001*
C^2	0.0356	1	0.0356	40.51	<0.0001*
D^2	0.0719	1	0.0719	81.87	<0.0001*
E^2	0.0084	1	0.0084	9.59	0.0044*
Residual	0.0246	28	0.0009		
Lack-of-fit	0.0231	26	0.0009	1.16	0.5651
Pure error	0.0015	2	0.0008		
Cor Total	1.76	44			
R^2			0.9861		
Adjusted R^2			0.9781		
Predicted R^2			0.9630		
Adequate precision			40.65		

* Significant.

of the decrease in RR198 concentration. It demonstrates the RR198 complete degradation or conversion into intermediate products under UV-LED irradiation in the presence of a photocatalyst.

Modeling and optimization

The RSM framework was used for modeling of UV-LED photocatalytic degradation of RR198 using TFNs through central composite experimental design. After evaluation, the quadratic polynomial to model showed the best prediction. The actual and predicted results are shown in Table 2. The final actual and coded equations were observed in Eqs. (3 and 4), which consist of 18 P-values calculated from the One-Way ANOVA (analysis of variance), by the 95% confidence interval.

$$\text{Decolorization} = -1.32012 - 0.001716{*}\text{RR198 Con.} + 0.096712{*}\text{pH} + 0.0087141{*}\text{TFNs} + 0.020751{*}\text{Time} + 1.00377{*}\text{PS} + 0.000968{*}\text{RR198 Con.}{*}\ \text{pH} + 0.000330{*}\text{RR198 Con.}{*}\ \text{TFNs} - 0.000054{*}\text{RR198 Con.}{*}\ \text{Time} - 0.003780{*}\text{pH} * \text{TFNs} - 0.000518{*}\text{pH} * \text{Time} - 0.031437{*}\text{pH} * \text{PS} - 0.000220{*}\text{RR198 Con.}^2 - 0.006539{*}\text{pH}^2 - 0.001491{*}\text{TFNs}^2 - 0.000132{*}\text{Time}^2 - 0.453281{*}\text{PS}^{2}{*}\ (3) \qquad \text{Eq. 3}$$

$$\text{Decolorization} = +0.5563 - 0.0855{*}A - 0.3446{*}B + 0.01094{*}C + 0.0907{*}D + 0.0959{*}E + 0.0774{*}AB + 0.0659{*}AC - 0.0431AD - 0.1512BC - 0.0828{*}BD - 0.0503{*}BE - 0.0882{*}A^2 - 0.1046{*}B^2 - 0.1491{*}\ C^2 - 0.2119{*}D^2 - 0.0725{*}E^2 \qquad \text{Eq. 4}$$

Where *Y* is the decolorization percentage of RR198, and other parameters were introduced in previous sections.

The results of ANOVA are represented in Table 3. According to the results, the nonlinear quadratic model would be appropriate due to the very low *P* value, which is smaller than 0.0001, and it led to a significant model. Furthermore, the lack-of-fit test was insignificance ($P = 0.5651$). It compares the residual error with the pure error from replicated design points. If residual error is greater than the pure error, then, the lack-of-fit test is significant, and therefore, the model could not be used.

Moreover, the coefficient of determination (R^2) value of 0.9861 is in reasonable agreement with the adjusted R^2 value of 0.9781, indicating an excellent agreement between the predicted and actual data. The predicted R^2 is equal to 0.9630, indicating that the proposed model has a high predictive capability for new observations. This could be illustrated in Figure 3A.

Also, the normal distribution plot of the studentized residuals was shown in Figure 3B. If this graph follows a linear trend, it shows that the distribution of errors is normal. The nonlinear trend emphasizes on abnormal error distribution. As a result, there will be a need to modify the design of experiments or re-examine the responses. As shown in Figure 3B, the studentized residuals have a normal distribution, and the error variance is homogeneous. Figure 3C represents the Cook's distance against the run number. Cook's distance is used to assess the influence of single or sets of observations in the RSM model. The higher the Cook's distance, the greater the impact of its observation. Generally, the Cook's distance greater than 1.0 or separated from the rest are influential data and should be eliminated. Therefore, based on Figure 3C, there is no observation that was excessively insignificant on the model. Furthermore, the adequate precision value of the proposed model was 40.65. Ratios greater than 4 indicate adequate model discrimination (27,28).

In the RSM model, the 3D plots could be used for response surfaces visualization to monitor the response variations with respect to two variables and keep fixed other variables. In Figures 4A to 4D, the model response can be seen. In Figure 4E, the optimum points of the studied variables were introduced via the numerical optimization module in Design-Expert software.

Figure 4A represents the dye concentration vs. pH; it shows that the RR198 decolorization increased enormously by decreasing the pH value at all investigated

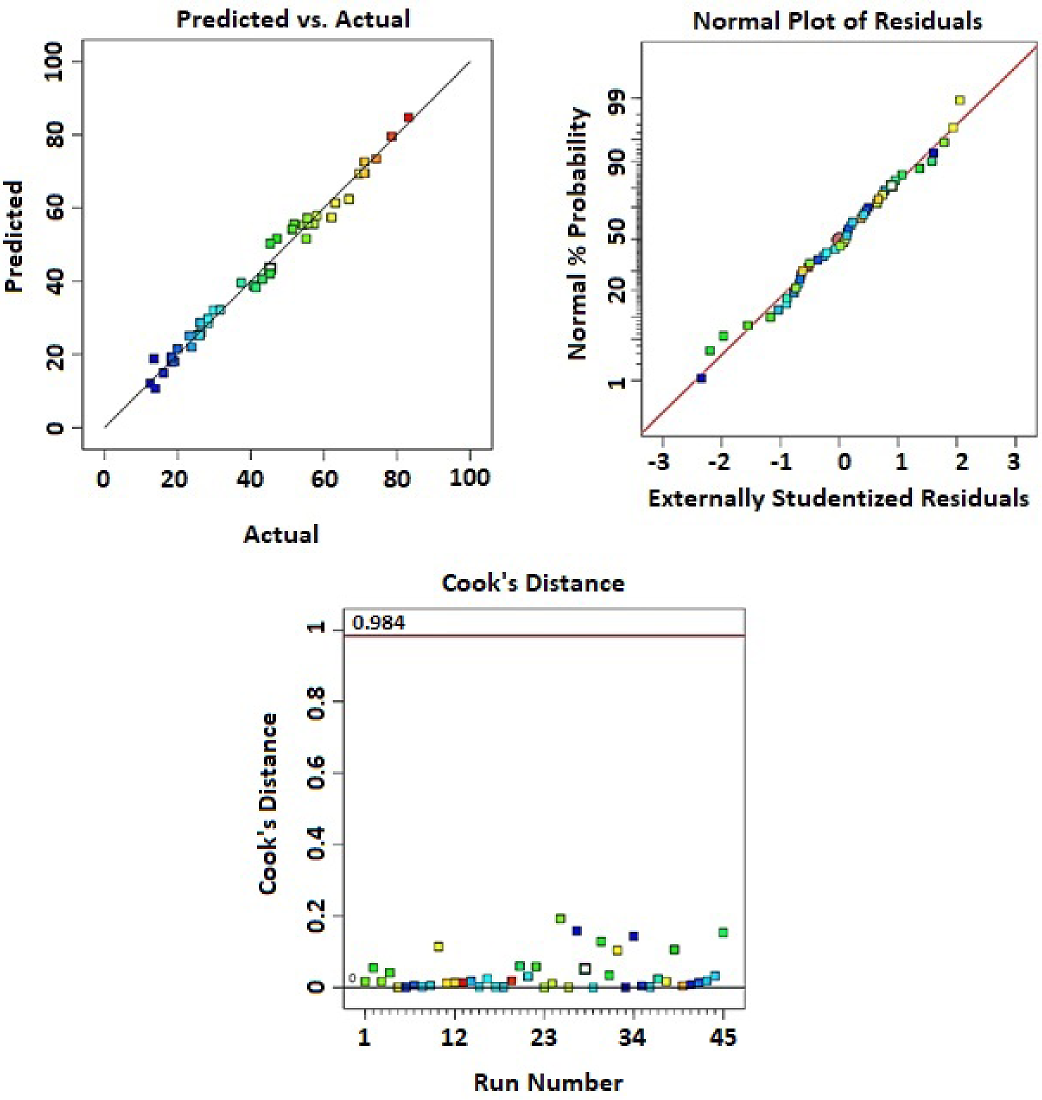

Figure 3. Diagnostic plots in the output of RSM model

dye concentrations. It emphasizes that the decolorization efficiency is highly affected by pH (29). According to other research, the adsorption has an important effect on photocatalytic degradation of azo dyes, especially when the TiO_2-based photocatalyst is used (13). The results of this study indicated that RR198 adsorbed on TFNs at acidic pH, because the adsorbent surface has a positive charge, and the anionic dye is well absorbed due to electrostatic attractions (30). Based on Figure 4E, the optimum RR198 degradation efficiency occurred at pH 3.0-4.25. Kaur et al. investigate the photocatalytic degradation of RR198 using N, Fe codoped TiO_2 nanoparticles under visible light and pointed out that at pH 3, the maximum dye removal occurred (31).

As shown in Figure 4B, the RR198 removal was gradually decreased with the increase in initial concentration of dye from 10 to 50 regardless of TFNs dosage. Also, with increasing TFNs, the decolorization efficiency increased sharply and TFNs coupled with UV-LED could degrade RR198 significantly through the photocatalytic decomposition mechanism. In addition, with increasing the TFNs dosage, the photon absorption on the surface of the catalyst was increased, which led to accelerating the photocatalytic degradation of RR198 (15,32). The optimum decolorization is observed at TFNs catalyst dosage in the range of 0.19-0.3 g/L (Figure 4E). However, more increase in catalyst dosage led to an increase in turbidity and a decline in light penetration and increasing in scattering effect, thereby, reducing the degradation efficiency (33).

In Figure 4C, the variations of efficiency as a function of time and dye concentration are visible. It is clear that by increasing the reaction time, the decolorization efficiency was increased regardless of the initial dye concentration. After reaching equilibrium time, the maximum decolorization efficiency was achieved, and it did not change anymore. The equilibrium time at different initial concentrations of dye was reached at 62-85 minutes. In a research conducted by Zazouli et al, the reaction time for photocatalytic degradation of Brilliant Blue FCF by

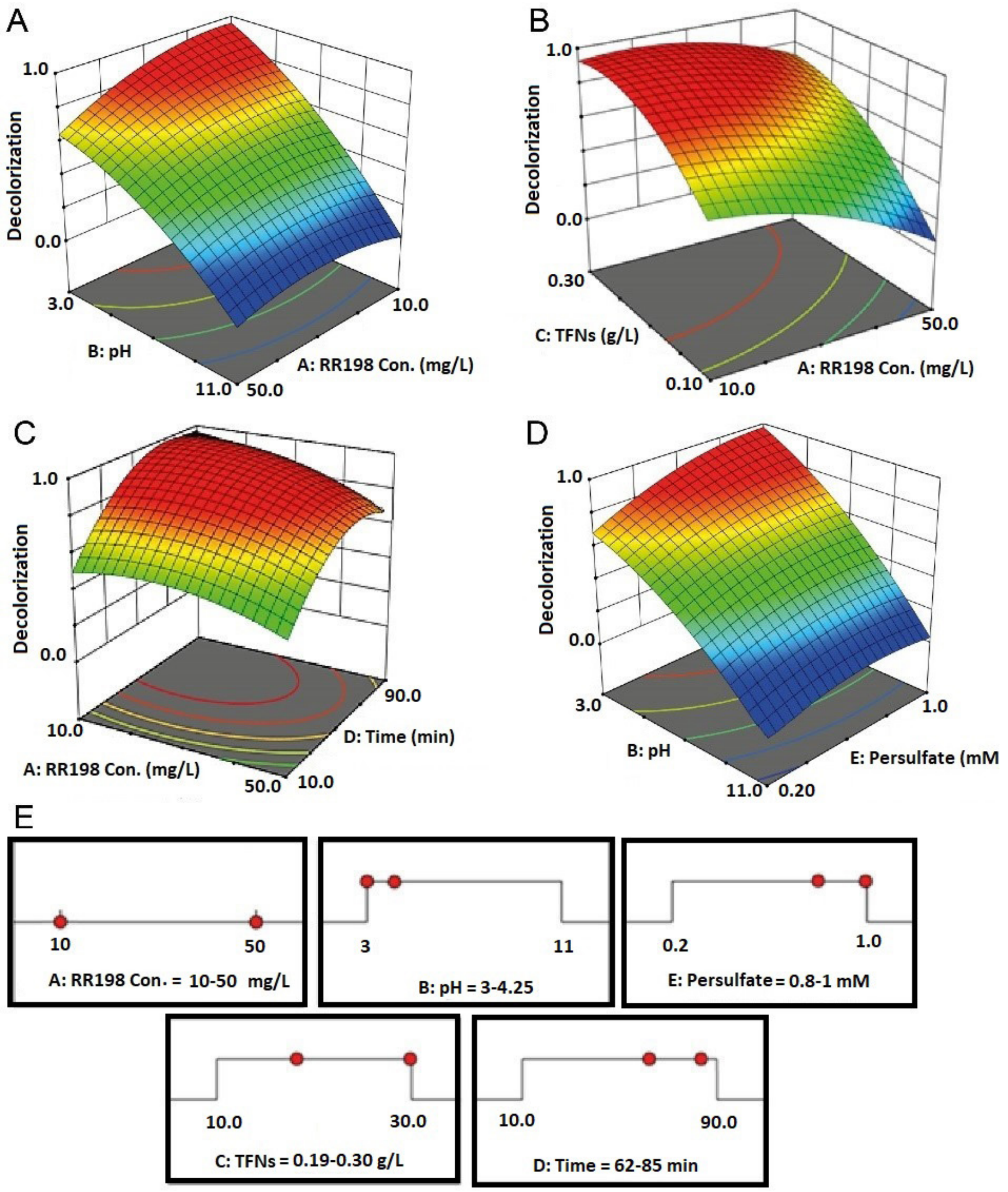

Figure 4. 3D graphs of RSM prediction showing the interaction effects of (A) pH and Ci-RR198, (B) TFNs and Ci-RR198, (C) Time and Ci-RR198, (D) pH and PS on the decolorization rate, and (E) optimization of the studied variables

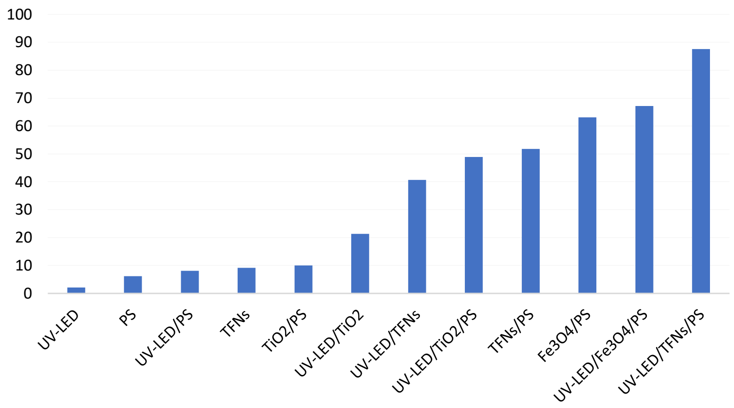

Figure 5. Degradation rate of RR198 in different conditions (pH = 3, RR198 concentration = 50 mg/L, reaction time = 90 min).

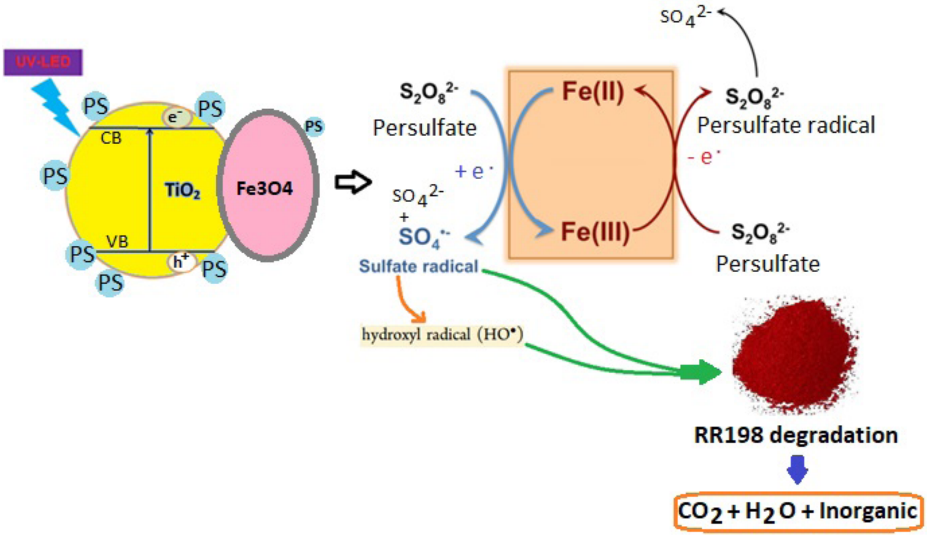

Figure 6. The mechanism of free radical production in the UV-LED/TFNs/PS system

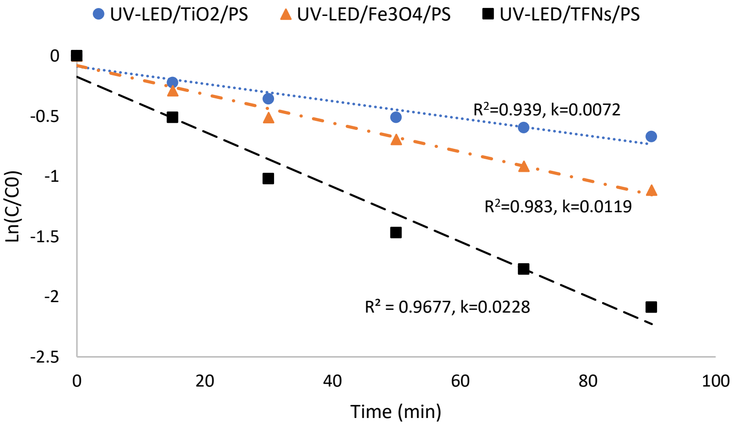

Figure 7. The linear regression of pseudo-first-order reaction kinetics (Photocatalyst = 0.3 g/L, pH = 3, Initial concentration = 50 mg/L, Time = 90 min)

Table 4. Comparison of different photocatalytic processes in the removal of dyes

Process	Removal efficiency (%)	Mineralization (%)	Time (min)	Reference
UV-LED/TFNs/PS	98.1	61.1	62	This study
CNS-SiO_2@TiO_2	75	-	90	(20)
TiO_2 P25	99	74	120	(21)
UV/ZnO	-	70-80	240	(22)
TiO_2	88.78	76.95	90	(23)
ZnO modified on activated carbon	96	-	60	(24)

Fe_3O_4–TiO_2 nanoparticles in the presence of PMS and UV sources was considered 60 minutes (15).

Figure 4D represents the effects of PS ion dosage on decolorization efficiency. By increasing PS concentration, the removal efficiency increased. The following, more explanation at about how PS affects the process. The optimum molar concentration of PS was obtained about 0.8-1 Mm (Figure 4E). Du et al demonstrated that with 0.5 g/L TiO_2/g-C3N4 photocatalysts and 2 mM PS, TOC could be decreased approximately 82.5% in 60 min (34).

The mechanism, mineralization, kinetic, and reusability study

To better understand the photocatalytic decolorization mechanism of RR198, experimental studies using different catalysts were carried out, the results are shown in Figure 5. According to the results, using UV-LED, PS, UV-LED/PS, TFNs, and TiO_2/PS had no more than 10% decolorization and did not have enough ability to produce free radicals for RR198 degradation. In the mentioned processes, the dominant mechanism for decolorization was adsorption onto catalysts.

The decolorization efficiency using UV-LED/TiO_2 and UV-LED/TFNs photocatalysts was about 21.4% and 40.7%, respectively; because of the excitement of photocatalysts in the presence of UV-LED and HO• production, decolorization considerably increased. UV-LED/TFNs were able to remove RR198 somewhat higher through the photocatalytic mechanism. This is because of UV-LED light source was applied here with 395-400 nm wavelength, which could not effectively activate TiO_2 with band-gap typically of about 3.2 eV; while the higher reactivity of TFNs could be described by a band-gap of about 2.8 eV, so UV-LED wavelength was powered enough to activate TFNs (32,35).

UV-LED/TiO_2 with the synergetic effect of PS via conduction electrons and radical sulfate production, improved decolorization to 48.9%. The TFNS/PS, in the absence of UV-LED light, revealed 51.8% decolorization. Because of the presence of Fe_3O_4 nanoparticles on TiO_2, PS activation is accelerated via Fe (II)/Fe (III) cycle and produces sulfate radical. In addition, by increasing pH, more sulfate radicals could be transformed to hydroxyl radicals (OH•) through the direct conversion of SO4•- in the hydrolysis reaction with H2O, based on Eqs. (5 and 6) (36). Furthermore, PS maybe decomposed by hole (h+) and generate S2O8•-, which is a weaker oxidant in comparison with SO4•- and HO• (37).

$$Fe^{2+} + S_2O_8^{2-} \rightarrow Fe^{3+} + SO_4^{-\circ} + SO_4^{2-} \qquad \text{Eq.5}$$

$$SO_4^{-\circ} + H_2O \rightarrow OH^{\circ} + HSO_4^{-} \qquad \text{Eq.6}$$

As shown in Figure 5, Fe_3O_4 nanoparticles and TFNs were applied for PS activation, separately. Fe_3O_4 could successfully catalyze PS and achieved 63.1% decolorization efficiency. The higher efficiency of the Fe_3O_4/PS compared with TFNs/PS denotes that Fe_3O_4 would be the principal agent for PS activation. Therefore, transition metals have an effective role in the powerful radical generation, which accelerating degradation efficiency. But the decolorization using Fe_3O_4/PS and UV-LED/Fe_3O_4/PS has no significant difference, because Fe_3O_4 has no photocatalytic activity. Eventually, UV-LED/TFNs/PS showed the highest catalytic activity for RR198 decolorization at 87.6% (36,38). Zazouli et al indicated that Fe_3O_4/TiO_2/PMS nano photocatalyst in the presence of UVA-LED completely decolorized Brilliant Blue FCF dye in 60 min reaction time. They demonstrated that UVA-LED/Fe_3O_4/TiO_2/PMS had higher efficiency than UVA-LED/Fe_3O_4/PMS and UVA-LED/TiO2/PMS (15). The mechanism of decolorization in UV-LED/TFNs/PS is illustrated in Figure 6.

The high decolorization from the solution does not mean complete mineralization of organic compounds. In this study, the dye mineralization during the degradation process is assessed through the TOC analysis. The mineralization of RR198 in initial concentrations of 10 and 50 mg/L during the optimum conditions (reaction time = 90 min, pH = 3, TFNs = 0.3 g/L, PS = 1.0 mM) were evaluated about 61.1% and 49.6%, respectively. Meanwhile, the decolorization efficiency in the same conditions was about 98.1% and 87.6%, respectively. The degree of mineralization was higher at lower initial concentrations and the same reaction time.

The effect of three main processes compared in this section (UV-LED/TiO_2/PS, UV-LED/Fe_3O_4/PS, and UV-LED/TFNs/PS) on the rate of RR198 decolorization were investigated at an initial RR198 concentration of 50 mg/L, pH 3, and photocatalyst of 0.3 g/L (Figure 7). By plotting Ln(C0/C) versus time, the decolorization rate constant (k) was obtained, the values of which were in agreement with pseudo first-order kinetics as confirmed by other researchers (15,17,39-41). Figure 7 represents that the k values for UV-LED/TiO_2/PS, UV-LED/Fe_3O_4/PS, and UV-LED/TFNs/PS processes were calculated at 0.0072, 0.0119, and 0.0228 min^{-1}, respectively. Obviously, the decolorization rate constant increased by using TFNs instead of Fe_3O_4 and TiO_2.

Kaur et al. investigated the photocatalytic degradation of RR198 using N, Fe codoped TiO_2 nanoparticles under visible light at initial concentration of 10 mg/L, pH 4.6, catalyst = 1.2 g/L, and the decolorization rate constant (k) was calculated 0.027 min^{-1} (31). Wu et al assessed the decolorization of RR198 in UV/TiO_2/$Na_2S_2O_8$ systems and the kinetic constants of photocatalytic degradation at initial concentration in the range of 10-80 mg/L, pH = 7, $Na_2S_2O_8$ = 0.5 mM, and TiO_2 = 0.5 g/L were obtained 0.0226-0.2424 min^{-1}.

Also, Table 4 compares different photocatalytic processes in the removal of dyes. The results show the acceptable performance of the method studied in this research for RR98 dye.

For the economical application of photocatalysts, the reusability of them has always been a concern. Hence, decolorization experiments of RR198 solution with initial concentration of 50 mg/L was performed in the presence of UV-LED/TFNs/PS (TFNs 0.3 g/L, PH 3, PS 1 mM, and reaction time 90 minutes). After each cycle, the TFNs were separated with a magnet and washed five times using distilled water, then, dried in the oven at 103°C for 1 hours. This process was repeated for 5 cycles in the same conditions. In each cycle, the initial concentration of dye was kept constant. The decolorization efficiency in the first to the fifth cycles was equal to 87.6%, 86.2%, 83.3%, 76.9%, and 67.1%. Generally, the decolorization gradually decreased with a steeper slope. This could be a result of two main reasons, first, the formation of intermediate complexes on the surface of photocatalyst, which prevent the PS activation and free radical production, and second, ferric or ferrous ion leaching from Fe_3O_4 nanoparticles, which led to the reduction of iron content in the photocatalysts. Despite the declining trend of decolorization, after 4 cycles, the total degradation efficiency has dropped by about 10%. Therefore, it could be concluded that the TFNs are reusable nanocomposite photocatalyst that supports four cycles of use (15).

Conclusion

In the present study, a TiO_2-Fe_3O_4 nanocomposite catalyst was synthesized and investigated for photocatalytic decolorization of RR198 solution under UV-LED irradiation in the presence of persulfate, which can act as an electron acceptor. The results of FTIR, XRD, FE-SEM, EDX and UV-Vis absorption analyzes showed that TFN nanocomposite was successfully synthesized. The results revealed that the TFNs photocatalyst has a good ability to degrade RR198 dye under visible light. Modeling and optimization through RSM demonstrated the maximum decolorization of RR198 at an initial concentration of 10-50 mg/L was reached under UV-LED irradiation of 62-85 min, PS = 0.8-1 mM, 0.19-0.3 g/L TFNs, and pH = 3. According to the results, the nonlinear quadratic model would be appropriate due to the very low P-value, which is lower than 0.0001 and it led to significant model. Furthermore, the lack-of-fit test reveals insignificance ($P = 0.5651$). Also, the coefficient of determination (R^2) value of 0.9861 is in reasonable agreement with the adjusted R^2 value of 0.9781, which demonstrates an excellent agreement between the predicted and actual data. The kinetics of the process was in agreement with pseudo-first-order. The k-values for UV-LED/TiO_2/PS, UV-LED/Fe_3O_4/PS, and UV-LED/TFNs/PS processes was calculated to be 0.0072, 0.0119, and 0.0228 min^{-1}, respectively. The mineralization of RR198 at initial concentrations of 10 and 50 mg/L under the optimum conditions were determined about 61.1% and 49.6%, meanwhile, the decolorization efficiency in the same conditions was about 98.1% and 87.6%, respectively. Furthermore, the reusability assessment demonstrated that TFNs are reusable nanocomposite photocatalysts, which support four use cycles with a 10% reduction in efficiency.

Acknowledgments

This article is the result of a research project approved by Isfahan University of Medical Sciences (IUMS). The authors would like to acknowledge Vice Chancellor for Research of IUMS for the financial support, Research Project, # 198121.

Authors' contribution

Conceptualization: Somayeh Rahimi.
Data curation: Somayeh Rahimi.
Formal analysis: Farzaneh Mohammadi.
Funding acquisition: Farzaneh Mohammadi.
Investigation: Maryam Mohammadi.
Methodology: Farzaneh Mohammadi, Somayeh Rahimi.
Project administration: Farzaneh Mohammadi.
Resources: Farzaneh Mohammadi.
Software: Farzaneh Mohammadi.
Supervision: Farzaneh Mohammadi.
Validation: Farzaneh Mohammadi.
Visualization: Farzaneh Mohammadi.
Writing – original draft: Farzaneh Mohammadi, Soudabeh Ghodsi, Hossein Karimi, Maryam Mohammadi.
Writing – review & editing: Farzaneh Mohammadi, Soudabeh Ghodsi, Hossein Karimi, Maryam Mohammadi.

Competing interests

None.

Ethical issues

Ethical code received from Vice Chancellor for Research of IUMS (IR.MUI.RESEARCH.REC.1398.490).

References

1. Ilyas M, Ahmad W, Khan H, Yousaf S, Yasir M, Khan A. Environmental and health impacts of industrial wastewater effluents in Pakistan: a review. Rev Environ Health. 2019;34(2):171-86. doi: 10.1515/reveh-2018-0078.
2. Zhang W, Zhang Y. Development of ZnFe2O4 nanoparticle functionalized baker's yeast composite for effective removal of methylene blue via adsorption and photodegradation. J Water Process Eng. 2020;37:101234. doi: 10.1016/j.jwpe.2020.101234.
3. El Amri A, Kadiri L, Hsissou R, Lebkiri A, Wardighi Z, Rifi EH, et al. Investigation of *Typha latifolia* (TL) as potential biosorbent for removal of the methyl orange anionic dye in the aqueous solution. Kinetic and DFT approaches. J Mol Struct. 2023;1272:134098. doi: 10.1016/j.molstruc.2022.134098.
4. Katheresan V, Kansedo J, Lau SY. Efficiency of various recent wastewater dye removal methods: a review. J Environ Chem Eng. 2018;6(4):4676-97. doi: 10.1016/j.jece.2018.06.060.
5. Song J, Huang M, Jiang N, Zheng S, Mu T, Meng L, et al. Ultrasensitive detection of amoxicillin by TiO2-g-C3N4@AuNPs impedimetric aptasensor: fabrication, optimization, and mechanism. J Hazard Mater. 2020;391:122024. doi: 10.1016/j.jhazmat.2020.122024.
6. Rahmani AR, Masoumi Z, Shabanlo A, Akbari S, Zolghadr Nasab H, Almasi H. Investigation of sonochemical oxidation process in the presence of SiO2, CuSO4 and Na2SO4 in removal of acid black1 azo dye from aqueous solution. J Rafsanjan Univ Med Sci. 2015;13(12):1115-28. [Persian].
7. Samadi A, Ahmadi R, Hosseini SM. Influence of TiO2-Fe3O4-MWCNT hybrid nanotubes on piezoelectric and electromagnetic wave absorption properties of electrospun PVDF nanocomposites. Org Electron. 2019;75:105405. doi: 10.1016/j.orgel.2019.105405.
8. Amiri-Hosseini S, Hashempour Y. Photocatalytic removal of malachite green dye from aqueous solutions by nano-composites containing titanium dioxide: a systematic review. Environ Health Eng Manag. 2021;8(4):295-302. doi: 10.34172/ehem.2021.33.
9. Lee J, von Gunten U, Kim JH. Persulfate-based advanced oxidation: critical assessment of opportunities and roadblocks. Environ Sci Technol. 2020;54(6):3064-81. doi: 10.1021/acs.est.9b07082.
10. Horikoshi S, Serpone N. Can the photocatalyst TiO2 be incorporated into a wastewater treatment method? Background and prospects. Catal Today. 2020;340:334-46.

doi: 10.1016/j.cattod.2018.10.020.

11. Mohammadi F, Bina B, Amin MM, Pourzamani HR, Yavari Z, Shams MR. Evaluation of the effects of AlkylPhenolic compounds on kinetic parameters in a moving bed biofilm reactor. Can J Chem Eng. 2018;96(8):1762-9. doi: 10.1002/cjce.23115.
12. Zhou Z, Liu X, Sun K, Lin C, Ma J, He M, et al. Persulfate-based advanced oxidation processes (AOPs) for organic-contaminated soil remediation: a review. Chem Eng J. 2019;372:836-51. doi: 10.1016/j.cej.2019.04.213.
13. Wei X, Xu X, Yang X, Li J, Liu Z. Visible light degradation of reactive black-42 by novel Sr/Ag-TiO2@g-C3N4 photocatalyst: RSM optimization, reaction kinetics and pathways. Spectrochim Acta A Mol Biomol Spectrosc. 2020;228:117870. doi: 10.1016/j.saa.2019.117870.
14. Mirshahghassemi S, Aminzadeh B, Torabian A, Afshinnia K. Optimizing electrocoagulation and electro-Fenton process fortreating car wash wastewater. Environ Health Eng Manag. 2017;4(1):37-43. doi: 10.15171/ehem.2017.06.
15. Zazouli MA, Ghanbari F, Yousefi M, Madihi-Bidgoli S. Photocatalytic degradation of food dye by Fe3O4–TiO2 nanoparticles in presence of peroxymonosulfate: the effect of UV sources. J Environ Chem Eng. 2017;5(3):2459-68. doi: 10.1016/j.jece.2017.04.037.
16. Alexpandi R, Abirami G, Murugesan B, Durgadevi R, Swasthikka RP, Cai Y, et al. Tocopherol-assisted magnetic Ag-Fe3O4-TiO2 nanocomposite for photocatalytic bacterial-inactivation with elucidation of mechanism and its hazardous level assessment with zebrafish model. J Hazard Mater. 2023;442:130044. doi: 10.1016/j.jhazmat.2022.130044.
17. Ding X, Gutierrez L, Croue JP, Li M, Wang L, Wang Y. Hydroxyl and sulfate radical-based oxidation of RhB dye in UV/H2O2 and UV/persulfate systems: kinetics, mechanisms, and comparison. Chemosphere. 2020;253:126655. doi: 10.1016/j.chemosphere.2020.126655.
18. Kaur R, Kushwaha JP, Singh N. Electro-oxidation of amoxicillin trihydrate in continuous reactor by Ti/RuO2 anode. Sci Total Environ. 2019;677:84-97. doi: 10.1016/j.scitotenv.2019.04.339.
19. Ajami S, Mohammadi M. Telemedicine against CoVID-19 crisis. Health Policy Technol. 2020;9(3):277-8. doi: 10.1016/j.hlpt.2020.05.002.
20. Olya ME, Vafaee M, Jahangiri M. Modeling of acid dye decolorization by TiO2–Ag2O nano-photocatalytic process using response surface methodology. J Saudi Chem Soc. 2017;21(6):633-42. doi: 10.1016/j.jscs.2015.07.006.
21. Mansor MR, Mustafa Z, Fadzullah SH, Omar G, Salim MA, Akop MZ. Recent advances in polyethylene-based biocomposites. In: Sapuan SM, Ismail H, Zainudin ES, eds. Natural Fibre Reinforced Vinyl Ester and Vinyl Polymer Composites. Woodhead Publishing; 2018. p. 71-96. doi: 10.1016/b978-0-08-102160-6.00003-2.
22. Galedari M, Mehdipour Ghazi M, Mirmasoomi SR. Photocatalytic process for the tetracycline removal under visible light: presenting a degradation model and optimization using response surface methodology (RSM). Chem Eng Res Des. 2019;145:323-33. doi: 10.1016/j.cherd.2019.03.031.
23. Dash G, Sen S, Pradhan RK, Ghosh S, Josileen J, Jayasankar J. Modeling framework for establishing the power law between length and weight of fishes and a meta-analysis for validation of LWRs for six commercially important marine fishes from the northwestern Bay of Bengal. Fish Res. 2023;257:106496. doi: 10.1016/j.fishres.2022.106496.
24. Jun LY, Karri RR, Yon LS, Mubarak NM, Bing CH, Mohammad K, et al. Modeling and optimization by particle swarm embedded neural network for adsorption of methylene blue by jicama peroxidase immobilized on buckypaper/polyvinyl alcohol membrane. Environ Res. 2020;183:109158. doi: 10.1016/j.envres.2020.109158.
25. Maruthapandi M, Eswaran L, Luong JHT, Gedanken A. Sonochemical preparation of polyaniline@TiO2 and polyaniline@SiO2 for the removal of anionic and cationic dyes. Ultrason Sonochem. 2020;62:104864. doi: 10.1016/j.ultsonch.2019.104864.
26. Kaur N, Kaur S, Singh V. Preparation, characterization and photocatalytic degradation kinetics of Reactive Red dye 198 using N, Fe codoped TiO2 nanoparticles under visible light. Desalin Water Treat. 2016;57(20):9237-46. doi: 10.1080/19443994.2015.1027956.
27. Eskandarian MR, Rasoulifard MH, Fazli M, Ghalamchi L, Choi H. Synergistic decomposition of imidacloprid by TiO2-Fe3O4 nanocomposite conjugated with persulfate in a photovoltaic-powered UV-LED photoreactor. Korean J Chem Eng. 2019;36(6):965-74. doi: 10.1007/s11814-018-0230-1.
28. Anwer H, Mahmood A, Lee J, Kim KH, Park JW, Yip AC. Photocatalysts for degradation of dyes in industrial effluents: opportunities and challenges. Nano Res. 2019;12(5):955-72. doi: 10.1007/s12274-019-2287-0.
29. Du X, Bai X, Xu L, Yang L, Jin P. Visible-light activation of persulfate by TiO2/g-C3N4 photocatalyst toward efficient degradation of micropollutants. Chem Eng J. 2020;384:123245. doi: 10.1016/j.cej.2019.123245.
30. Sri Kunarti E, Kartini I, Syoufian A, Widyandari KM. Synthesis and photoactivity of Fe3O4/TiO2-Co as a magnetically separable visible light responsive photocatalyst. Indones J Chem. 2018;18(3):403-10. doi: 10.22146/ijc.26831.
31. Pervez MN, He W, Zarra T, Naddeo V, Zhao Y. New sustainable approach for the production of Fe3O4/graphene oxide-activated persulfate system for dye removal in real wastewater. Water. 2020;12(3):733. doi: 10.3390/w12030733.
32. Liu H, Bruton TA, Li W, Van Buren J, Prasse C, Doyle FM, et al. Oxidation of Benzene by persulfate in the presence of Fe(III)- and Mn(IV)-containing oxides: stoichiometric efficiency and transformation products. Environ Sci Technol. 2016;50(2):890-8. doi: 10.1021/acs.est.5b04815.
33. Xie E, Zheng L, Li X, Wang Y, Dou J, Ding A, et al. One-step synthesis of magnetic-TiO2-nanocomposites with high iron oxide-composing ratio for photocatalysis of rhodamine 6G. PLoS One. 2019;14(8):e0221221. doi: 10.1371/journal.pone.0221221.
34. Ertugay N, Acar FN. Removal of COD and color from Direct Blue 71 azo dye wastewater by Fenton's oxidation: kinetic study. Arab J Chem. 2017;10(Suppl 1):S1158-S63. doi: 10.1016/j.arabjc.2013.02.009.
35. Mittal H, Alhassan SM, Ray SS. Efficient organic dye removal from wastewater by magnetic carbonaceous adsorbent prepared from corn starch. J Environ Chem Eng. 2018;6(6):7119-31. doi: 10.1016/j.jece.2018.11.010.
36. Amin MM, Bina B, Ebrahimi A, Yavari Z, Mohammadi F, Rahimi S. The occurrence, fate, and distribution of natural and synthetic hormones in different types of

wastewater treatment plants in Iran. Chin J Chem Eng. 2018;26(5):1132-9. doi: 10.1016/j.cjche.2017.09.005.

37. Yang J, Xu X, Liu Y, Gao Y, Chen H, Li H. Preparation of SiO2@TiO2 composite nanosheets and their application in photocatalytic degradation of malachite green at emulsion interface. Colloids Surf A Physicochem Eng Asp. 2019;582:123858. doi: 10.1016/j.colsurfa.2019.123858.
38. Santos LM, de Amorim KP, Andrade LS, Batista PS, Trovó AG, Machado AE. Dye degradation enhanced by coupling electrochemical process and heterogeneous photocatalysis. J Braz Chem Soc. 2015;26(9):1817-23. doi: 10.5935/0103-5053.20150158.
39. Almeida Guerra WN, Teixeira Santos JM, Raddi de Araujo LR. Decolorization and mineralization of reactive dyes by a photocatalytic process using ZnO and UV radiation. Water Sci Technol. 2012;66(1):158-64. doi: 10.2166/wst.2012.154.
40. Buyukada M. Prediction of photocatalytic degradation and mineralization efficiencies of Basic Blue 3 using TiO2 by nonlinear modeling based on Box-Behnken design. Arab J Sci Eng. 2016;41(7):2631-46. doi: 10.1007/s13369-016-2175-6.
41. Dargahi A, Samarghandi MR, Vaziri Y, Ahmadidoost G, Ghahramani E, Shekarchi AA. Kinetic study of the photocatalytic degradation of the acid blue 113 dye in aqueous solutions using zinc oxide nanoparticles immobilized on synthetic activated carbon. J Adv Environ Health Res. 2019;7(2):75-85. doi: 10.22102/jaehr.2019.163880.1117.